

## Article

# Feasible Parameters of Ohmic Areas of YBaCuO Thin Films Switched via Moving Unstable Border between Superconducting and Normal States

Linus Ardaravičius  and Oleg Kiprijanovič \* 

Center for Physical Sciences and Technology, Saulėtekio al. 3, LT-10257 Vilnius, Lithuania;  
linas.ardaravicius@ftmc.lt

\* Correspondence: oleg.kiprijanovic@ftmc.lt

**Abstract:** A system of two equations based on one of the classical electricity laws was used to determine the sizes and temperatures of ohmic areas formed under action of overcritical nanosecond electrical pulses. Calculations were performed at five points for three experimentally obtained voltage–current ( $V$ - $I$ ) dependences for samples with the same geometry but different critical current density values. The system included two additional conditions to satisfy the known descriptive model of transition from superconducting (SC) to a normal (N) state—S-N switching—and to obtain physically acceptable solutions over the entire current range of  $V$ - $I$  dependence. The solution for each point takes the form of a function, since the initial temperature increase of the primary channel across the film is entered as a parameter. Two modes of concentrated energy release in the channel were disclosed. Their random appearance leads to an unexpected degradation of the sample. As such, the obtained results correspond to the situations occurring during the experiments. The validity of applying additional conditions to the system is discussed. In the discussion, it is also explained at which moments the moving S-N border acquires the velocity of the order of  $\sim 10^6$  m/s, comparable to the Fermi velocity. Consideration to describe the moving unstable S-N border as being constantly in a state of Richtmyer–Meshkov instability is presented.

**Keywords:** HTSC thin films; nanosecond electrical pulses; S-N switching; switched N areas; Fermi velocity; Richtmyer–Meshkov instability



**Citation:** Ardaravičius, L.; Kiprijanovič, O. Feasible Parameters of Ohmic Areas of YBaCuO Thin Films Switched via Moving Unstable Border between Superconducting and Normal States. *Coatings* **2024**, *14*, 266. <https://doi.org/10.3390/coatings14030266>

Academic Editor: Aomar Hadjadj

Received: 9 January 2024

Revised: 14 February 2024

Accepted: 21 February 2024

Published: 22 February 2024



**Copyright:** © 2024 by the authors. Licensee MDPI, Basel, Switzerland. This article is an open access article distributed under the terms and conditions of the Creative Commons Attribution (CC BY) license (<https://creativecommons.org/licenses/by/4.0/>).

## 1. Introduction

Created with great effort, the superconducting (SC) state can be easily damaged by an increased temperature or applied magnetic field. Despite this, work on creating materials with a  $T_c$  above the room temperature does not stop. Recently, information about the material LK-99 appeared, exciting the scientific community [1]. Additional research is being carried out to clarify the SC properties of similar materials. The applied magnetic field is an important tool to quantify the properties of the SC state [2].

Since 1986, high-temperature superconductors have been appearing in which the SC state is formed at a liquid nitrogen temperature of 77 K, and these, including YBaCuO, are type-II superconductors. When they are in an SC mixed state with a transport current, magnetic flux quanta (vortices) move under the influence of the Lorentz force perpendicularly to the current, and this movement causes the appearance of a voltage drop [3]. A detailed review systematizing results on the fast vortex motion was published recently [4]. Experimental investigations of superconductor properties at the microlevel are performed using time-resolved precise THz spectroscopy. The response signals are analyzed after the excitation of superconductors using ultra-short laser pulses. A comprehensive review of the methodology and obtained results are presented in paper [5].

Theoretical investigations that elucidate the properties of superconductors at the microlevel are carried out intensively, judging by publications. Nowadays, low-dimensional

SC structures are of particular interest. Comprehensive results in the study of various effects during the transition of such structures to a non-equilibrium state, including resistive ones, are obtained by applying the time-dependent Ginzburg–Landau equations. The excitation of a superconductor cylindrical nanowire using a THz pulse causes the order parameter to perform a damped oscillation [6]. The resistive state created by an applied voltage in narrow SC channels is characterized by oscillating phase-slip centers forming [7]. Paper [8] introduces pyTDGL, a Python package that solves a generalized time-dependent Ginzburg–Landau equation for two-dimensional superconductor samples of an arbitrary geometry, allowing the author to simulate vortex and phase-slip dynamics in SC thin film devices.

By the end of the 20th century, the number of experiments and publications on the transition of the SC state to the normal (N) state using both current and optical pulses (S–N switching) of high-temperature superconductors decreased noticeably. Apparently, the obtained data were deemed sufficient to focus on practical applications instead [9]. Theoretically, a thermomagnetic shock wave is predicted during the sudden disruption of the SC state, even for type-I superconductors [10]. Nonlinear dynamic disruption of the mixed state can be accompanied by the appearance of thermomagnetic shock waves propagating through the vortex lattice [11]. Non-equilibrium magnetic flux penetration can form a magnetic flux shock wave [12]. Calculated velocities of these SC state disrupting waves can reach  $10^3$  m/s. Recently, a publication appeared where the properties of slow shock waves in microscopic magnetic lattices were experimentally investigated. This investigation used desktop-scale modeling of a tunable magnetic lattice [13].

In thin films, the current is nonhomogeneous through the cross-section, concentrating at the film edges. Quantitatively, the edge magnetic field penetration is characterized by the Pearl length  $\lambda_{\text{eff}}$  [14,15], and this current filament of high density becomes the S–N border of  $\lambda_{\text{eff}}$  width. Analysis of scanning electron microscope (SEM) images of thin YBaCuO films damaged by overcritical current pulses of a nanosecond duration revealed that the vortices do not overcome the edge barrier [16,17]. The results of the analysis of the SEM images are presented in the paper [18]. They show that the N zone propagates with the S–N border in bending instability and initially forms a narrow channel across the film. Such fast S–N border movement creates a resistive state in the channel for a very short time, and the interaction of a flowing current with this state forms an ohmic area.

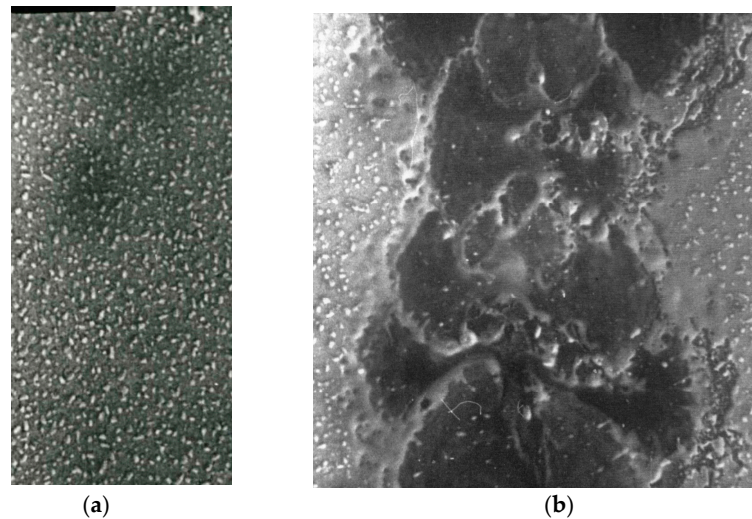
The paper [19] proposes a descriptive model of the S–N switching. In this model, the achievement of the critical current is characterized by the event that at the edges of the film, the current filaments enter a state of bending instability, a flat version of a screw one, classified as one of the magnetic hydrodynamic instabilities. Under the prevailing Lorenz force, acting on the current filament against the Meissner force, the N zones with unstable S–N borders begin to move towards the center, forming a 50–80  $\mu\text{m}$  width channel. Analogous to this is the constriction of a plasma cord in three-dimensional geometry. According to the model, the N zone propagation due to the forces' opposition occurs in a step-by-step manner with coherent jet generation. As proposed in the paper [18], the incompressible medium for forming the jets is SC Meissner currents. Thus, the shape of the S–N border changes at every step due to the unstable state, the formation of the jets with no mass transfer, and other magnetic hydrodynamic phenomena. At the same time, the mean velocity of the N zone propagation during the formation of the channel is as high as  $6.1 \times 10^5$  m/s, regardless of the forces' opposition.

It so happened that in papers [18,19] no attention was paid directly to the S–N switching. The sizes of the switched areas and their temperature after the switching were not considered. To eliminate this disadvantage, a two-equation system based on one of the classical electricity laws was used to estimate the geometric and temperature parameters of the switched ohmic areas. The propagation of the N zone has certain attributes of a detonation wave, and the S–N border has the capability to form coherent jets. The question is raised about the validity of the interpretation of the unstable S–N border movement as being constantly in a state of Richtmyer–Meshkov instability.

## 2. Known Data from Experimental Investigations

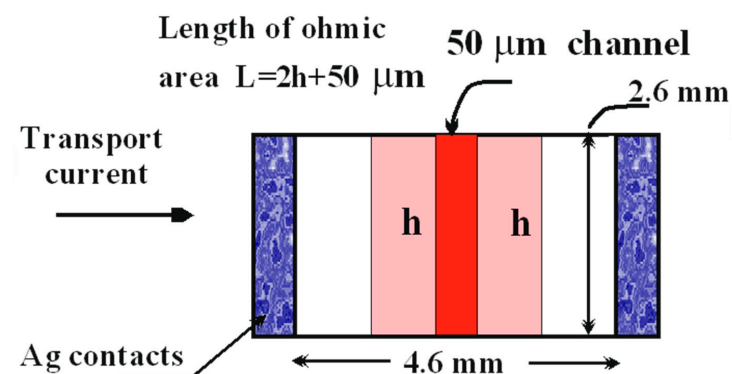
To determine the parameters of ohmic areas, some known data from experimental investigations were used.  $V$ - $I$  dependences of the wide, thin YBaCuO film samples were measured to define their critical and damage currents. Samples of the same geometry differing in the quality of the SC state, mainly by critical current, were used. More details of the experiments are described in the paper [18].

Figure 1a demonstrates an SEM image of a YBaCuO thin film with a 150 nm thickness deposited by a pulsed laser on MgO substrate. In Figure 1b, one can see that the melted channel appeared as a result of flowing current interaction with a resistive state created by the fast movement of the unstable S-N border. These visible melted shapes allowed us to draw at least some conclusions [19], since moving the S-N border forms this section within a hundred ps, and subsequent melting distorts the initial picture over much longer times.



**Figure 1.** YBaCuO thin film fabricated via pulsed laser deposition on MgO substrate; the SEM image dimensions are  $95 \times 45 \mu\text{m}^2$  (a). Irreversible film damage covering the initially formed channel; the SEM image dimensions are  $90 \times 85 \mu\text{m}^2$  (b).

In compliance with the descriptive model of the pulsed S-N switching proposed in the paper [19], the film is switched in two stages with the consequent appearance of ohmic areas. At the first stage, the pulse front heats up a narrow channel during  $2 \times 10^{-9}$  s. In the second stage, a pulse with a duration of 20 ns switches the area of length  $L$ , which includes the already partially heated channel. The schematic diagram of the sample with a switched area is presented in Figure 2. The sample was placed in the break of the microstrip line, which was connected by microstrip-to-cable transitions to the cables in the cryostat chamber.



**Figure 2.** Schematic diagram of YBaCuO film sample partly switched to ohmic state. The film is deposited on a 0.5 mm thick MgO substrate and has a thickness of 150 nm. Top view.

To calculate the switched ohmic areas, we are setting the channel width to 50  $\mu\text{m}$ .  $V$ - $I$  dependences of three samples are presented in Figure 3. Marked on these dependences are the points entered into the system to calculate the parameters of switched areas.

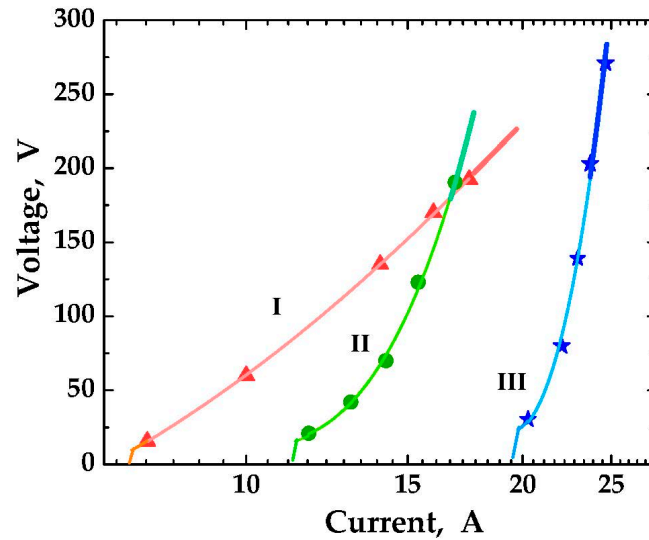


**Figure 3.**  $V$ - $I$  dependences of the samples differing in the quality of the SC state. The points at which calculations have been made are marked. Line thickening indicates the regions where unexpected damage is possible.

### 3. Equation System Based on Joule–Lenz Law to Find the Feasible Parameters of the Ohmic Areas

The sizes of switched areas and their temperature rise at marked points are the solution of the two-equation system based on the classical Joule–Lenz electricity law, as presented below in Equations (1) and (2):

$$\left[ R_{chan}^{T_c} (1 + \alpha_{\rho el} \cdot \Delta T_{chan}) + R_{2h}^{T_c} \right] \cdot (1 + \alpha_{\rho el} \cdot \Delta T_L) = R_n \tag{1}$$

Equation (1) includes the term of the channel resistance increase at the first stage, followed by the increase in resistance of the whole ohmic area with the temperature rise during the second stage. Here,  $R_{chan}^{T_c}$  is the channel resistance just after  $T$  reaches  $T_c$ . It is obtained using the standard formula and inserting the resistivity value from Table 1.

**Table 1.** Some physical and electrical parameters of YBaCuO films used in calculations.

Sample	I	II	III
$T_c$ (K)	85	89	90
$j_c$ (A/cm <sup>2</sup> )	$2 \times 10^6$	$3 \times 10^6$	$5.2 \times 10^6$
$\rho_{el}$ ( $\Omega \cdot \text{m}$ ) at $T_c$	$1.8 \times 10^{-6}$	$1 \times 10^{-6}$	$9 \times 10^{-7}$
$\lambda_{\text{eff}}$ ( $\mu\text{m}$ )	3.1	1.54	1.155
$\rho$ (kg/m <sup>3</sup> )	$6.3 \times 10^3$	$6.3 \times 10^3$	$6.3 \times 10^3$
$\alpha_{\rho el}$ (1/K)	$3.2 \times 10^{-2}$	$3.2 \times 10^{-2}$	$3.2 \times 10^{-2}$

The same applies to resistance  $R_{2h}^{T_c}$ . The resistance temperature coefficient  $\alpha_{\rho el}$ , is also taken from Table 1. The standard value of the YBaCuO resistivity is  $3 \times 10^{-6} \Omega \cdot \text{m}$  at 100 K, but it lowers a bit near  $T_c$ . Also, as a rule, the resistivity decreases with an increasing film quality. These resistivity values can be found in Table 1. The initial channel temperature

rise  $\Delta T_{chan}$  is entered as a parameter because we have no means of estimating at least some definitive values of this rise.

$$\frac{c_n \cdot \rho \cdot V_{chan} \cdot \Delta T_{chan}}{2 \times 10^{-9}} + \frac{c_n \cdot \rho \cdot V_L(L) \cdot \Delta T_L}{\tau_{pulse}} = I_n^2 \cdot R_n \quad (2)$$

Equation (2) includes the pulse power dissipation terms. The first term defines what part of the power dissipates in the channel during the pulse front, while the other defines what part dissipates in the whole ohmic area during the 20 ns pulse. Here,  $\rho$  is specific weight and  $V_{chan}$  and  $V_L$  are the film volumes of the channel and the whole switched area, correspondingly. In Table 1 are also presented critical temperature, critical current, and  $\lambda_{eff}$  values for the samples. Common values are the YBaCuO specific weight and temperature resistance coefficient.

The length  $L$  of the switched ohmic area and the area temperature rise  $\Delta T_L$  are the obtained system solutions. Final temperatures of switched channels are obtained by summing  $T_c$ ,  $\Delta T_{chan}$ , and  $\Delta T_L$ . The solution of the system was carried out using the Mathcad software package. Physically unacceptable solutions are discarded.

#### 4. Obtained Results

The length  $L$  is graphically presented in Figures 4–6 as a function of the initial switched channel temperature. In Figure 4, a linear growth of the length  $L$ , depending on the temperature for the first points of all three dependences, is evident. The final temperatures of the channels do not cause concern regarding the film damage since their values are not high enough.

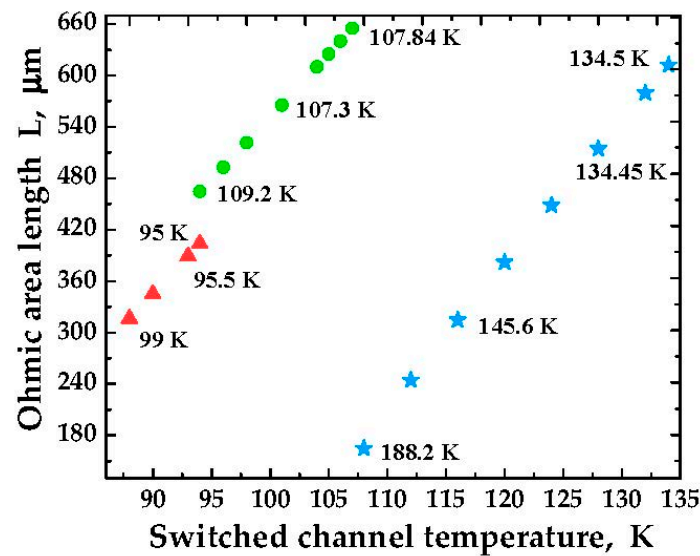
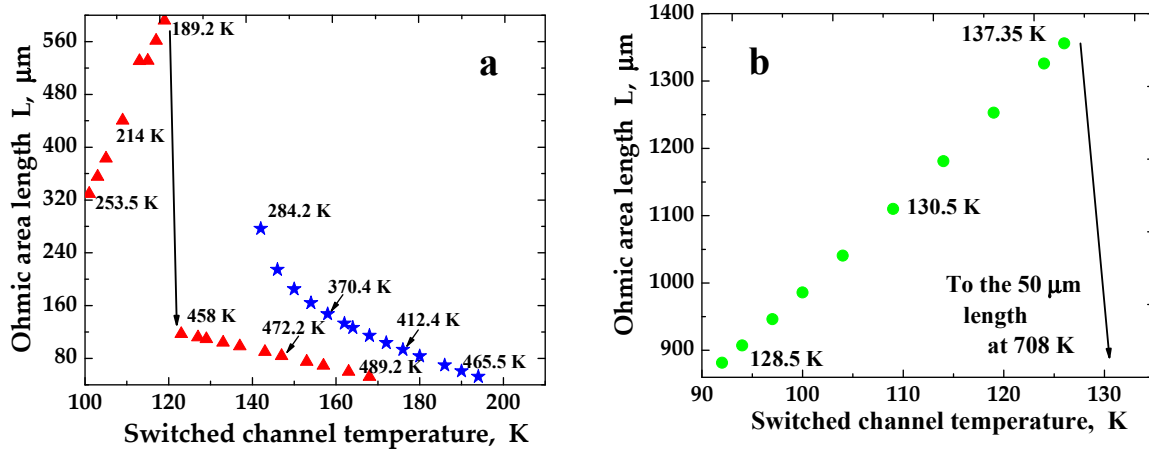


**Figure 4.** Growth of length  $L$  vs. switched channel temperature for the first points of all dependences. Temperature values inside the plot indicate the final temperatures of the channels. Triangles, circles, and stars correspondingly mark the first, second, and third dependences.

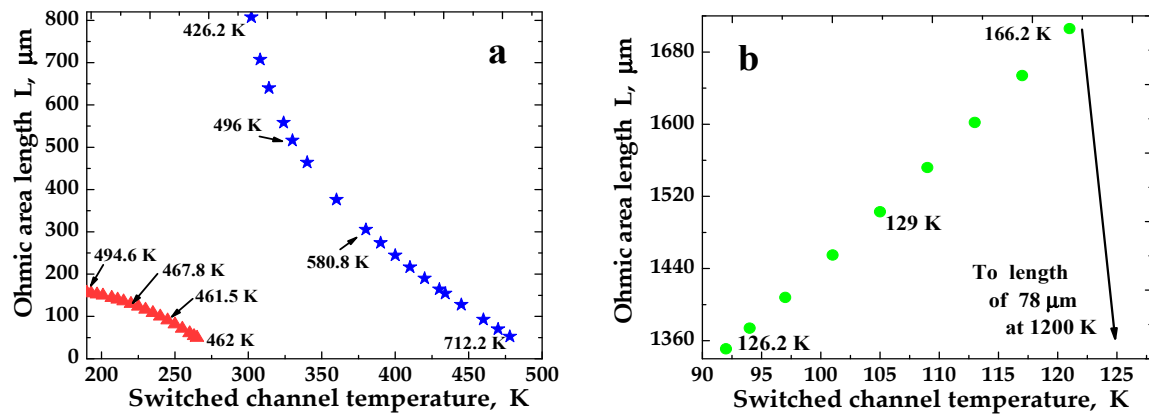
We prefer to place the third point functions of all dependences in a single figure; however, the second dependence has values significantly larger than the first one, and it is placed separately in Figure 5b. The function of the third point of the third dependence cannot be compactly placed with the function of the first dependence because its argument values are too large. Instead, the  $L$  vs. channel temperature function for the second point is set in Figure 5a because its course is similar to the third point function.

Figure 5 shows how the growing linear mode, presented in Figure 4, changes for the functions of the first, second, and third dependences. In Figure 5a, the function for the first dependence undergoes a sharp drop, indicated by an arrow, after which a concentration of

pulse energy is observed. After the drop, the length  $L$  converges from 110  $\mu\text{m}$  to 50  $\mu\text{m}$  if the switched channel temperature increases up to 170 K and, therefore, the channel absorbs all power. Such an energy release can be called a mode of converging energy concentration. The final heating temperature of the channel is about 482.2 K, indicating possible film damage, but the probability of such an event is still very low. For the second point of the third dependence, a drop in the function is absent, and the concentration of the pulse energy is also observed. This narrowing channel absorbs all power if the initial switched channel temperature increases to 193 K.



**Figure 5.** The length  $L$  vs. switched channel temperature for the third point of the first dependence and the second point of the third one (a). The length  $L$  vs. switched channel temperature for the third point of the second dependence (b). Temperature values inside the plots indicate the final temperatures of the channels. Triangles, circles, and stars correspondingly mark the first, second, and third dependences.



**Figure 6.** The length  $L$  vs. switched channel temperature for the fifth point of the first dependence and for the fifth point of the third one (a). The length  $L$  vs. switched channel temperature for the fifth point of the second dependence (b). Temperature values inside the plots indicate the final temperatures of the channels. Triangles, circles, and stars correspondingly mark the first, second, and third dependences.

The function of the second dependence in Figure 5b also undergoes a sharp drop if the switched temperature increases only up to 128 K. Still, after the drop, length  $L$  immediately becomes 50  $\mu\text{m}$ , equaling the channel length. Since the temperature of irreversible damage to the film is about 700 K, it follows that after this drop the sample will finally be damaged. The energy concentration just after the drop can be defined as a mode of abrupt energy concentration, in contrast to the converging one.

Figure 6 demonstrates the function courses for the fifth points of the first, second, and third dependences. As shown in Figure 6a, the functions of the first and third dependences no longer have common argument values. The function of the first dependence does not have a drop, and it passes in the mode of the energy concentration in which the 50  $\mu\text{m}$  channel finally absorbs all power. The final temperatures of the channels are close to 470 K and indicate that they are in a condition near to damaging. The function of the third dependence is again in the converging mode. High final temperatures of the areas with a decreasing  $L$  below 500  $\mu\text{m}$  indicate that film damaging processes are likely to occur (see Figure 6a). Surprisingly, the function of the second dependence (see Figure 6b) still shows further linear  $L$  growth and has a sharp drop to the immediate channel length of 78  $\mu\text{m}$ . At the point after the drop, there is a considerable increase in temperature to 1200 K, indicating the abrupt damaging mode.

## 5. Discussion

The question may arise why, when describing the quantities entered in the system, the specific heat capacity  $c$  value is not indicated. As one can see,  $c$  is entered into the system with the index  $n$ . That is, each marked point of the current–voltage dependences has its own  $c_{mn}$  value. It becomes evident that if the standard 200 J/(kg·K)  $c$  value for volumetric YBaCuO is entered into Equation (2), no physically acceptable solutions will be obtained, excluding the first point of the first dependence.

In our thin film case, very intense energy dissipation occurs because of the local overcritical current concentration and current concentration due to a cumulative effect. Even in paper [19], estimation of the irreversible film damage processes, observed in SEM images, required the  $c$  value to be 300 J/(kg·K). Linearly increasing  $c_{mn}$  depending on the current increase, which also corresponds to the increase in the current in the filament, we obtain physically acceptable system solutions. Figure 7 shows the growth in  $c_{mn}$  values that gives acceptable results.

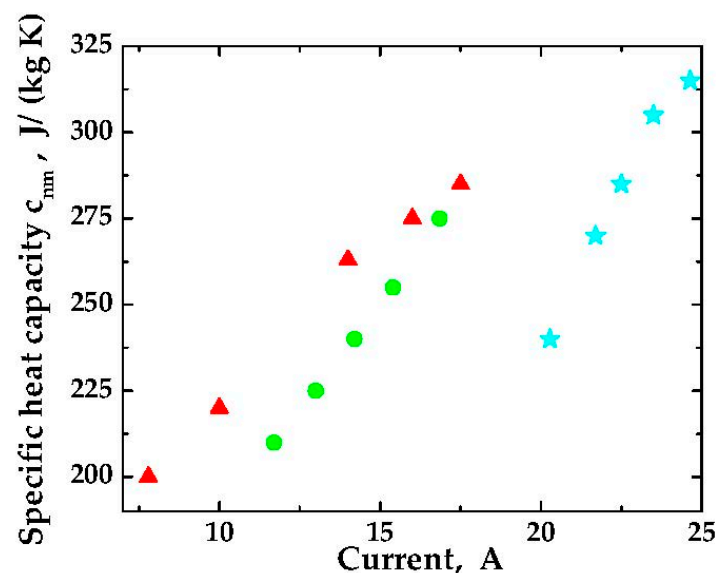


Figure 7. Increase in  $c_{mn}$  at  $c$  vs. current plot used for solving of the system. Triangles, circles, and stars correspondingly mark the first, second, and third dependences.

As one can see, when the proposed system accounts for the power released at the pulse front and the increasing value of the specific heat capacity, it becomes possible to obtain solutions that explain the results observed in the experiment. Qualitatively, the solutions also include modes that lead to random film damage, up to their irreversible damage. For the first dependence, this is the mode with energy concentration in the channel (see Figure 5a). After the drop, the channel width narrows to 50  $\mu\text{m}$ , while temperature growth

can induce the film damage at the third point. For the second dependence, the mode of concentration is not observed, and the linear increase in  $L$  can suddenly end in a drop into a region with a width comparable to the channel width. So, because of the high temperature, irreversible damage of the region is possible after the third point (see Figure 5b), but the probability of such an event is low and not yet known. The third dependence, like the first, demonstrates the mode of energy concentration, and the damage is possible already at the second point, while the irreversible damage at the fifth point is probable (see Figure 5a).

In paper [19], the mean velocity of the propagation of the S-N border was estimated from experimental data, and during the formation of the channel it is  $6.1 \times 10^5$  m/s. This velocity is greater than the detonation one. It is necessary to clarify where this value comes from. According to the descriptive model, the N zone propagation process is a step-by-step process. The dynamics of the steps are presented in paper ([19], Table 4). At the first stage, when Lorentz and Meissner forces act, there is a relatively slow development of bending instability, and the amplitudes of the bulges increase. At the second stage, the development stagnates in an unstable equilibrium. And then, at the third shortest stage, the macroscopic SC state “decides” to take a new position of the S-N border for the sake of its protection. This is a line between the maxima of the nearby bulges. It is at this moment of the local disappearance of the Meissner currents and correspondingly the Meissner force that the valley buckles with velocity comparable to the Fermi velocity. Indeed, the disappearance of the energy gap occurs without mass transfer and the movement of the S-N border on a micron scale can occur at such a large velocity [20,21]. During the buckling, a coherent jet is formed, and until it reaches the line between nearby bulges, its velocity will correspond to the velocity calculated for the air–water border [19]. But when it goes beyond the line, Meissner’s force will again provide strong resistance to it. However, in our case it is difficult to formulate a criterion for the lossless velocity, similar to the Landau criterion, which is sometimes used for type-I superconductors [22]. Using the distances between the bulges,  $13 \mu\text{m}$  and  $6 \mu\text{m}$  for the first and third cases ([19], Figure 2) and buckling times of 5.5 and 2.6 ps, correspondingly ([19], Table 4), one can obtain the velocity values of the Fermi ones. So, such step-by-step propagation of the N zone with coherent jet formation at the S-N border obtains the mean velocities of the order  $10^5$  m/s.

An inspection of unstable conditions at interfaces between media with different properties leads us, among others, to the Richtmyer–Meshkov instability. It manifests when a shock wave passes through the boundary of gases or liquids with different properties creating conditions for their mixing [23–25]. This is a single action, and it would seem to have nothing to do with our N zone propagation. According to the model, the N zone propagates by discrete steps, and part of the current energy is spent to maintain the temperature increase. At each step, the S-N border takes a different shape due to its unique properties, which allow the border to be considered as an independent object [18,19]. All these circumstances urge us to consider such movement of an unstable S-N border as being in a state of Richtmyer–Meshkov instability at each step.

## 6. Conclusions

A theoretical investigation of the S-N switching of type-II SC YBaCuO thin films through ns electrical pulses was carried out. The equation system based on one of the classical electricity laws was solved. Two additional conditions had to be applied for obtaining physically acceptable solutions to determine the geometric and temperature parameters of the switched areas. The converging and abrupt modes of the energy concentration in a narrow channel across the film, which can lead to unexpected film damage or destruction, were revealed. This corresponds to the situations occurring during experimental studies on the S-N switching. A deep coupling between the microscopic and macroscopic behavior of the SC state has been revealed. The macroscopic state, protecting its boundaries, instantly reacts to a threat and, on a microscopic scale, moves its Meissner border with Fermi velocity to a more convenient position. This explains how, despite the opposite action of the Lorentz and Meissner forces, the mean velocity of the N zone propagation during the formation of

the narrow channel can reach  $6.1 \times 10^5$  m/s. An attempt is made to consider describing the moving unstable S-N border as being constantly in a state of Richtmyer–Meshkov instability.

**Author Contributions:** Methodology, O.K.; Investigation, O.K.; Writing—original draft, O.K.; Writing—review & editing, L.A. and O.K. All authors have read and agreed to the published version of the manuscript.

**Funding:** This research received no external funding.

**Institutional Review Board Statement:** Not applicable.

**Informed Consent Statement:** Not applicable.

**Data Availability Statement:** Data are contained within the article.

**Conflicts of Interest:** The authors declare no conflict of interest.

## References

- Lee, S.; Kim, J.; Im, S.; An, S.; Kwon, Y.-W.; Ho, A.K. Consideration for the development of room-temperature ambient-pressure superconductor (LK-99). *J. Korean Cryst. Growth Cryst. Technol.* **2023**, *33*, 61–70. [\[CrossRef\]](#)
- Schrieffer, J.R. Theories of high temperature superconductivity. In Proceedings of the VIII-th International Conference on Megagauss Magnetic Field Generation and Related Topics, Tallahassee, FL, USA, 18–23 October 1998; Schneider-Muntau, H.J., Ed.; World Scientific Publishing Co., Pte. Ltd.: Singapore, 2004; pp. 39–45.
- Dew-Hughes, D. The critical current of superconductors: An historical review. *Low Temp. Phys.* **2001**, *27*, 713–722. [\[CrossRef\]](#)
- Dobrovolskiy, O. Fast dynamics of vortices in superconductors. *Encycl. Condens. Matter Phys.* **2024**, *2*, 735–754. [\[CrossRef\]](#)
- Demsar, J. Non-equilibrium phenomena in superconductors probed by femtosecond time-domain spectroscopy. *J. Low Temp. Phys.* **2020**, *201*, 676–709. [\[CrossRef\]](#)
- Zachmann, M.; Croitoru, M.D.; Vagov, A.; Axt, V.M.; Papenkort, T.; Kuhn, T. Ultrafast terahertz-field-induced dynamics of superconducting bulk and quasi-1D samples. *New J. Phys.* **2013**, *15*, 55016. [\[CrossRef\]](#)
- Yerin, Y.S.; Fenchenko, V.N. Dynamics of the resistive state of a narrow superconducting channel in the ac voltage driven regime. *Low Temp. Phys.* **2013**, *39*, 1023–1031. [\[CrossRef\]](#)
- Horn, L.B. pyTDGL: Time-dependent Ginzburg–Landau in Python. *Comput. Phys. Commun.* **2023**, *291*, 108799. [\[CrossRef\]](#)
- Vertelis, V.; Stankevič, T.; Balevičius, S.; Stankevič, V.; Žrauskienė, N.; Plaušinitienė, V.; Tolvaišienė, S.; Schneider, M.; Šimkevičius, Č. Superconducting protector against electromagnetic pulses based on YBCO film prepared on an Al<sub>2</sub>O<sub>3</sub> substrate with a CeO<sub>2</sub> sublayer. *Supercond. Sci. Technol.* **2021**, *34*, 035007. [\[CrossRef\]](#)
- Maksimov, I.L. Thermomagnetic shock waves in hard superconductors. *J. Phys. D Appl. Phys.* **1988**, *21*, 251–254. [\[CrossRef\]](#)
- Tailanov, N.A. Thermomagnetic shock waves in the vortex state in type-II superconductors. In *Topics in Superconductivity Research*; Martins, B.P., Ed.; Nova Science Publishers: Hauppauge, NY, USA, 2005; pp. 37–59.
- Deutsch, E.; Shapiro, B.Y.; Shapiro, I. Magnetic flux shock wave and hydrodynamic dendritic instability in type-II superconducting film. *Phys. C* **2008**, *468*, 23–30. [\[CrossRef\]](#)
- Li, J.; Chockalingam, S.; Cohen, T. Observation of Ultraslow Shock Waves in a Tunable Magnetic Lattice. *Phys. Rev. Lett.* **2021**, *127*, 014302. [\[CrossRef\]](#) [\[PubMed\]](#)
- Pearl, J. Current distribution in superconducting films carrying quantized fluxoids. *Appl. Phys. Lett.* **1964**, *5*, 65–66. [\[CrossRef\]](#)
- Prokof'ev, D. Distribution of the magnetic field induced by a current passing through slabs in the superconducting and normal states. *Tech. Phys.* **2006**, *51*, 675–682. [\[CrossRef\]](#)
- Bin, C.P.; Livingston, J.D. Surface barrier in type-II superconductors. *Phys. Rev. Lett.* **1964**, *12*, 14–17. [\[CrossRef\]](#)
- Bezuglyj, A.I.; Shklovskij, V.A.; Budinská, B.; Aichner, B.; Bevez, V.M.; Mikhailov, M.Y.; Vodolazov, D.Y.; Lang, W.; Dobrovolskiy, O.V. Vortex jets generated by edge defects in current-carrying superconductor thin strips. *Phys. Rev. B* **2022**, *105*, 214507. [\[CrossRef\]](#)
- Kiprijanovič, O.; Ardaravičius, L.; Gradauskas, J.; Šimkevičius, Č.; Keršulis, S.; Ašmontas, S. Instability, magnetic flux trapping and cumulative effect during pulsed S-N switching of thin high quality YBaCuO films. *Supercond. Sci. Technol.* **2020**, *33*, 095013. [\[CrossRef\]](#)
- Kiprijanovič, O.; Ardaravičius, L. Descriptive model of the transition from superconducting to normal state in thin high quality YBaCuO films by nanosecond electrical pulses. *Thin Solid Films* **2022**, *748*, 139159. [\[CrossRef\]](#)
- Sobolewski, R. Quasiparticle thermalization and recombination in high-temperature superconductors excited by femtosecond optical pulses. In *New Developments in High-Temperature Superconductivity*; Klamut, J., Veal, B., Dabrowski, B., Klamut, P., Kazimierski, M., Eds.; Springer: Berlin/Heidelberg, Germany, 2000; pp. 100–122. [\[CrossRef\]](#)
- Bobyrev, Y.V.; Petnikova, V.M.; Rudenko, K.V.; Shuvalov, V.V. Spectral, temporal and temperature features of the nonlinear response of high-temperature superconductors in transient nonlinear spectroscopy. *Quantum Electron.* **2006**, *36*, 895–917. [\[CrossRef\]](#)

22. Baym, G.; Pethick, C.J. Landau critical velocity in weakly interacting Bose gases. *Phys. Rev. A* **2012**, *86*, 023602. [[CrossRef](#)]
23. Jacobs, J.W.; Sheeley, J.M. Experimental study of incompressible Richtmyer–Meshkov instability. *Phys. Fluids* **1996**, *8*, 405–415. [[CrossRef](#)]
24. Zhou, Y. Rayleigh–Taylor and Richtmyer–Meshkov instability induced flow, turbulence, and mixing. II. *Phys. Rep.* **2017**, *723–725*, 1–160. [[CrossRef](#)]
25. Zhou, Y.; Williams, R.J.; Ramaprabhu, P.; Groom, M.; Thornber, B.; Hillier, A.; Mostert, W.; Rollin, B.; Balachandar, S.; Powell, P.D.; et al. Rayleigh–Taylor and Richtmyer–Meshkov instabilities: A journey through scales. *Phys. D* **2021**, *423*, 132838. [[CrossRef](#)]

**Disclaimer/Publisher’s Note:** The statements, opinions and data contained in all publications are solely those of the individual author(s) and contributor(s) and not of MDPI and/or the editor(s). MDPI and/or the editor(s) disclaim responsibility for any injury to people or property resulting from any ideas, methods, instructions or products referred to in the content.